Citation: von Engeln, A., G. Nedoluha, and G. Kirchengast, Deviation from a Hydrostatic Atmosphere in Radio Occultation Data, in Occultations for Probing Atmosphere and Climate (G. Kirchengast, U. Foelsche, A.K. Steiner, eds.), pp. 119-126, Springer, Berlin-Heidelberg, 2004.

Deviation from a Hydrostatic Atmosphere in Radio Occultation Data

A. von Engeln[1], G. Nedoluha[2], and G. Kirchengast[3]

[1] George Mason University Fellow at the Naval Research Laboratory, Washington, D.C., USA
engeln@uni-bremen.de
[2] Naval Research Laboratory, Washington, D.C., USA
[3] Institute for Geophysics, Astrophysics, and Meteorology, University of Graz, Austria

Abstract. A 1D Var sensitivity study of simulated radio occultation measurements is presented. Temperature and water vapor profiles are retrieved, along with a reference pressure to generate the pressure profile by applying the hydrostatic equation. High resolution European Center for Medium Range Weather Forecasts (ECMWF) atmospheric fields are used with a ray tracing tool to calculate the exact positions of the tangent point. The atmospheric profiles following the calculated tangent points trajectory in the 3D ECMWF fields are used to simulate bending angle measurements with a 1D forward model. Assimilation of these bending angles in a 1D Var tool employing the same 1D forward model is performed. We analyze the sensitivity of the retrieval to the assumption of hydrostatic equilibrium for a non-vertical atmospheric scan. Deviations of more than 1 % from a hydrostatic pressure profile can occur for certain mid-latitude and polar conditions. The effect upon the retrieval capabilities is usually negligible except for the most extreme cases.

1 Introduction

The radio occultation measurement technique is for example described in [5]. Most of the early retrievals of temperature and water vapor profiles from radio occultation measurements were focusing on a direct retrieval approach. We focus on a 1D Var approach that allows the simultaneous determination of these profiles along with a reference pressure. We use simulated radio occultation measurements made from a single LEO satellite on May 19, 2001. About 550 GPS occultation events were found and a subset of 110 was used in this study. Measurements were simulated using a ray tracing model and a high resolution ECMWF dataset to determine the exact tangent point trajectory. The primary purpose of this study is to provide quantitative assessments of the errors caused by the hydrostatic approximation which is generally used in

retrieving atmospheric parameters from GPS occultation measurements. Results presented here are a subset of a more thorough study already presented in [1].

2 Forward Model Setup

Two forward models have been used in this study, a 3D ray tracing tool, and a 1D forward model. Within the 3D ray tracing tool, ECMWF atmospheric analysis fields with 4 time steps, 60 vertical levels, and a T511 horizontal resolution (about 39 km) [6, 9, 3] were used to determine the tangent points of the rays. We calculate bending angles using a 1D forward model, with the temperature and water vapor values taken from the ECMWF fields at the tangent point trajectory.

The 3D ray tracer model used here is part of the End-to-end GNSS Occultation Performance Simulator tool [4]. It derives the actual tangent point trajectory in the 3D ECMWF fields. The ray trace terminates when one of the rays hit the Earth's surface, thus not all occultations reach down to the surface. Almost all of the 110 simulated occultations reach tangent altitudes ≤ 5 km, but only about 30 reach tangent altitudes < 1 km.

The 1D forward model used in this study neglects the effects of atmospheric horizontal variations. The principle equations of the radio occultation 1D forward model are given in [5]; the calculation of the bending angle as a function of refractivity follows an Abelian integral equation, refractivity itself depends on pressure, temperature, and water vapor. 1D ECMWF profiles following the tangent point trajectory as determined by the 3D ray tracer model are used within this model.

Table 1 summarizes the bending angle errors and the sampling (reflecting the resolution) of the measurement. We assumed reasonable error characteristics which are in-between the "proof-of-concept" GPS/MET instrument [5] and expected accuracies of modern receivers [2]. Useful determination of bending angles above 60 km is not possible, due to the poor signal-to-noise ratio of mesospheric radio occultation data.

Table 1. Sampling grid used for the simulated measurements, along with the corresponding bending angle errors assumed.

Height [km]	Sampling dz [km]	Error [μrad]
$00 \leq z \leq 25$	0.25	4.0
$25 \leq z \leq 40$	0.50	2.8
$40 \leq z \leq 60$	1.00	2.0

3 Retrieval Model

The retrieval algorithm used here is based on the 1D Var or Optimal Estimation Method [8]. It uses a priori knowledge on the state of the atmosphere to constrain the solution, where an a priori equals true sceanario is used over here. We retrieve the temperature profile between 0 km and 100 km, the water vapor profile between 0 km and 20 km, and a reference pressure from which the hydrostatic atmospheric pressure profile is generated. The reference pressure is usually retrieved at the lowest retrieval altitude. The vertical retrieval grid is given in Table 2.

Table 2. Vertical retrieval grid.

Parameters	Height [km]	Sampling dz [km]
Temperature	$00 \leq z \leq 30$	0.5
	$30 \leq z \leq 40$	1.0
	$40 \leq z \leq 60$	2.5
	$70 \leq z \leq 100$	10.0
Water Vapor	$00 \leq z \leq 20$	0.5

The a priori error covariance matrix is generated with a 2.5 K a priori uncertainty for temperatures up to 20 km and a linear increase up to 20 K at 100 km. We also assume a 40 % uncertainty in water vapor and a 1 % error in the reference pressure. Errors reflect in general Numerical Weather Prediction model short range forecast accuracies [7]. The measurement covariance matrix is generated with the errors presented in Table 1. A conservative approach for correlations (off-diagonal elements) in these matrices was taken, where both matrices are assumed to be diagonal (i.e., the measurement and the a priori profile are uncorrelated between different levels).

4 Horizontal Displacement of the Tangent Point

The latitude and longitude of the tangent point will generally change during an occultation event, caused by the motion of the satellites and by the variation of atmospheric refractivity with altitude. This horizontal displacement is, at high altitudes, mainly caused by changes in the occultation geometry, while at lower altitudes the atmospheric refraction provides the dominant contribution.

We separate the occultations in three latitude bands. The mean occultation latitude θ defines the latitude band as: tropical ($|\theta| < 30°$), mid-latitude ($60° > |\theta| > 30°$) and polar ($|\theta| > 60°$). The total number of occultations falling into a specific band is: tropical 45, mid-latitude 38, polar 27.

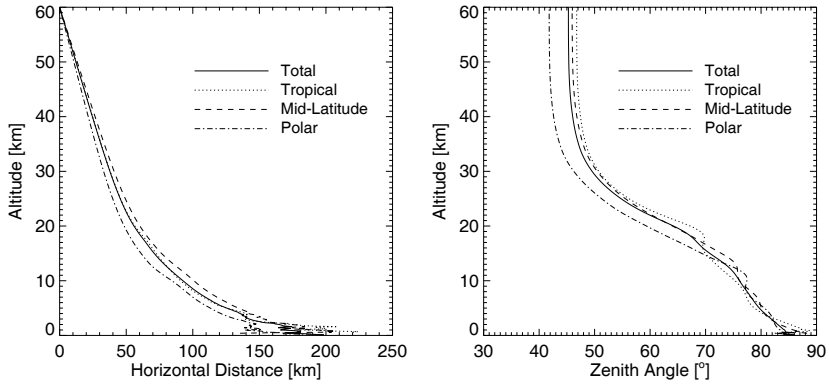

Fig. 1. Averaged horizontal displacement of tangent point (left) and zenith angle (right) for all 110 occultations, total and for different latitude bands. Noise has been removed from the zenith angle calculations by a 1 km boxcar average.

Figure 1 (left) shows the average horizontal displacement starting at a tangent altitude of 60 km. The geometric contribution varies linearly with altitude, it is about 80 km at the surface. The total horizontal displacement is around 200 km near the surface, with higher values found for tropical conditions, and lower ones for polar conditions. The average horizontal displacement at lower altitudes is underestimated since, just as for real observations, occultations in regions with low refractivity variations are more likely to reach lower altitudes in the ray tracing model, while strong variations will more often lead to a termination of the ray tracing process higher up in the atmosphere because the ray hits the Earth.

The zenith angle, defined as the angle between the local zenith and the line connecting successive tangent points of an occultation, is shown in Figure 1 (right). The zenith angle of the tangent point trajectory associated with a vertical scan would be 0°, but is found to be around 45° at altitudes around 60 km and increases to close to 90° at low altitudes. The zenith angles at higher altitudes are determined by the geometry of the observation. Polar occultations show lower zenith angles because the GPS orbit inclination is about 55° thus all observations are made toward the South or North. All occultations reach zenith angles around 85° independent of the latitude band at low altitudes, thus the scan at low altitudes is far from being vertical.

5 Deviations from a Hydrostatic Atmosphere

The ECMWF fields are hydrostatic in the vertical, but due to the horizontal displacement of the tangent point discussed above, the resulting pressure

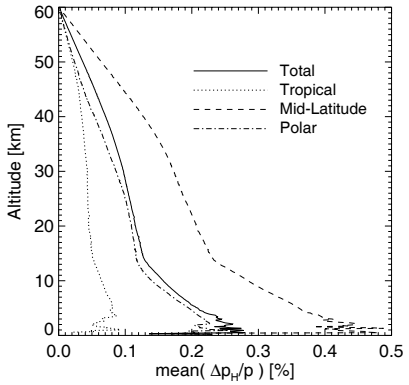

Fig. 2. Mean deviation ($\Delta p_{\mathrm{H}}/p$) from a hydrostatic pressure profile for all 110 occultations, total and for different latitude bands.

profile along the tangent point trajectory might deviate from the hydrostatic approximation.

To investigate the error introduced by assuming a hydrostatic atmosphere for GPS occultation measurements we first calculated a hydrostatic pressure profile using the 1D temperature and water vapor profiles following the tangent point trajectory in the 3D ECMWF fields. This hydrostatic pressure profile calculation was initialized with the pressure value found in the 3D ECMWF fields at 60 km. The hydrostatic pressure profile was then compared with the actual pressure at the tangent point locations in the 3D ECMWF fields. The percentage deviation of a pressure profile p_{H} calculated following the hydrostatic approximation from the actual pressure profile along the tangent point trajectory $p_{3\mathrm{D}}$ was calculated at each altitude level as:

$$(\Delta p_{\mathrm{H}}/p) = |(p_{\mathrm{H}} - p_{3\mathrm{D}})/p_{3\mathrm{D}}| \qquad [\%] \tag{1}$$

Figure 2 shows the mean of ($\Delta p_{\mathrm{H}}/p$) for all occultations and separated by latitude bands. The mean of ($\Delta p_{\mathrm{H}}/p$) over all occultation gradually increases with decreasing altitude and reaches a maximum of about 0.25 % near the surface. Minor deviations from the hydrostatic assumption appear for tropical conditions, with a mean of ($\Delta p_{\mathrm{H}}/p$) around 0.05 %. Mid-latitudes occultations experience larger deviations from a hydrostatic atmosphere, averaging more than 0.4 % near the surface. Deviations increase especially in the troposphere where strong temperature and water vapor gradients exist.

The maximum pressure deviation $max(\Delta p_{\mathrm{H}}/p)$ was calculated and sorted by value and occultation location to get a more quantitative picture. Table 3 lists the number of occultations falling within various $max(\Delta p_{\mathrm{H}}/p)$ intervals.

Out of the 110 occultations processed, most show only minor deviations from a hydrostatic atmosphere. Nevertheless there are a significant number

Table 3. Maximum deviations $max(\Delta p_H/p)$ from a hydrostatic atmosphere found over atmospheric pressure profile.

Deviation [%]	Total # of Occ	Latitude Band Tropical	Mid-Lat	Polar
$0.0 \leq max(\Delta p_H/p) < 0.1$	36	28	3	5
$0.1 \leq max(\Delta p_H/p) < 0.2$	30	12	9	9
$0.2 \leq max(\Delta p_H/p) < 0.3$	17	3	9	5
$0.3 \leq max(\Delta p_H/p) < 0.4$	9	2	3	4
$0.4 \leq max(\Delta p_H/p) < 0.5$	3	0	3	0
$0.5 \leq max(\Delta p_H/p) < 0.6$	5	0	2	3
$0.6 \leq max(\Delta p_H/p) < 0.7$	2	0	2	0
$0.7 \leq max(\Delta p_H/p) < 0.8$	3	0	3	0
$0.8 \leq max(\Delta p_H/p) < 0.9$	0	0	0	0
$0.9 \leq max(\Delta p_H/p) < 1.0$	0	0	0	0
$max(\Delta p_H/p) \geq 1.0$	5	0	4	1

of occultations (about 5 %) where pressure deviations of more than 1 % from the hydrostatic atmosphere appear. The maximum deviation is around 1.5 %. Generally $(\Delta p_H/p)$ increases almost linearly with distance from the initialization point at 60 km. The separation by latitude bands shows that tropical and polar occultations generally experience a pressure profile close to hydrostatic, while most of the severe deviations from hydrostatic appear at mid-latitudes.

The effect of such a non hydrostatic deviation on the temperature and water vapor retrieval is shown in Figure 3 for an occultation that experienced a severe deviation $max(\Delta p_H/p) = 1.5$ % from hydrostatic conditions. A calculation with an a priori equals the true is used, hence the difference between these two profiles is zero in both figures. Different altitudes for the reference pressure retrieval were evaluated, where the true pressure found in the p_{3D} profile at that particular altitude was used as a priori. An assessment of the retrieval capabilities (as given by the 1D Var total retrieval error covariance matrix) with different reference pressure retrieval altitudes showed only a negligible effect (not shown).

Severe deviations from a hydrostatic atmosphere can lead to significant retrieval errors. Maximum temperature errors of about 0.5 K are found for all reference pressure altitudes. The maximum error in water vapor reaches about 20 % for this occultation, where this is mainly caused by a strong water vapor gradient at around 3 km. Other occultations with similar deviations from the hydrostatic atmosphere exhibit errors of less than 10 % in water vapor.

The largest error in the retrieved reference pressure is almost 0.5 % for a reference altitude at 40 km. The smallest errors are generally found when we choose a reference altitude of around 20 km. This causes the hydrostatic deviations to be distributed to both lower and higher altitudes and thus minimizes the error at the reference pressure altitude.

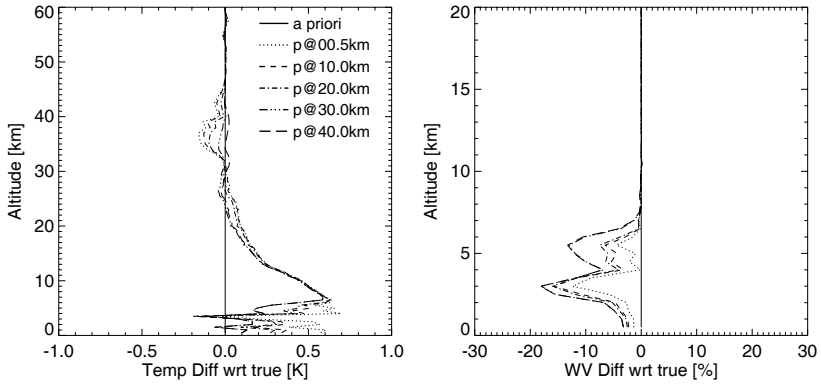

Fig. 3. Deviations from the true temperature (left) and water vapor (right) profile for a severe non hydrostatic atmosphere (Location 40.8° S, 56.4° W). Note: different height ranges.

Calculations with moderate deviations $max(\Delta p_{\mathrm{H}}/p) = 0.4\,\%$ show only a negligible error in the retrieval. The error introduced in the retrieved temperature and water vapor profile is very small, with a maximum error of about 0.1 K for temperature, and about 1.5 % for water vapor. The reference pressure error for this case is around 0.03 %.

6 Conclusions

We have presented a 1D Var sensitivity study of radio occultation measurements using 110 simulated occultations. A 3D ray tracing tool together with high resolution ECMWF fields was used to derive the actual tangent points of the occultation. The ECMWF atmospheric profiles following the tangent point is used in a 1D forward and 1D Var assimilation tool to investigate the effect of a non hydrostatic atmosphere upon the assimilation of radio occultation data. Atmospheric temperature, water vapor, and a reference pressure for the generation of a hydrostatic pressure profile are retrieved. The reference pressure was generally retrieved at the lowest retrieval altitude.

We calculated the horizontal displacement of the tangent point for a set of simulated occultations. We found that this displacement is usually around 200 km if one initializes the scan at an altitude of 60 km. On average, about 80 km of this displacement is caused by the satellite geometry, while the rest is due to atmospheric refraction. The zenith angle of the tangent point trajectory associated with a vertical scan would be 0°, but is found to be around 45° at altitudes around 60 km and increases to close to 90° at low altitudes.

The atmosphere along the tangent point trajectory deviates from hydrostatic conditions due to the horizontal displacement. Deviations usually reach

a maximum of about 0.2 %, but can reach values higher than 1 % for certain mid-latitude and polar conditions. The effect upon the retrieval capabilities is usually negligible except for the most extreme cases, where maximum errors of up to 0.5 K in temperature, 20 % in water vapor, and 0.5 % in the reference pressure were found.

Acknowledgments. This work was supported by an Internal Government Study from the Integrated Program Office of the National Polar-orbiting Operational Environmental Satellite System (NPOESS) and by the Office of Naval Research (ONR). The authors wish to thank Dr. N. Kreitz (ECMWF, Reading, UK) and Dr. S. Bühler (Institute of Environmental Physics, University of Bremen, Germany) for support with the ECMWF data extraction.

References

[1] von Engeln A, Nedoluha G, Kirchengast G, Bühler SA (2003) One-dimensional variational (1-D Var) retrieval of temperature, water vapor, and a reference pressure from radio occultation measurements: A sensitivity analysis. J Geophys Res 108(D11): 7-1 - 7-13, doi: 10.1029/2002JD002908

[2] ESA/EUMETSAT (1998) The GRAS instrument on METOP. ESA/EUMETSAT Rep ESA No. VR/3021/PI, EUM No. EPS/MIS/IN/9: 38 p., ESA/ESTEC, Noordwijk, Netherlands

[3] Jakob C, Andersson E, Beljaars A, Buizza R, Fisher M, Gerard E, Ghelli A, Janssen P, Kelly G, McNally AP, Miller M, Simmons A, Teixeira J, Viterbo P (2000) The IFS cycle CY21R4 made operational in October 1999. ECMWF Newsletter No 87: 2–9

[4] Kirchengast G, Fritzer J, Ramsauer J (2002) End-to-end GNSS Occultation Performance Simulator version 4 (EGOPS4) software user manual. Techn Rep ESA/ESTEC-3/2002: 472 pp., Inst for Geophys, Astrophys, and Meteorol, Univ of Graz, Austria

[5] Kursinski ER, Hajj GA, Schofield JT, Linfield RP, Hardy KR (1997) Observing Earth's atmosphere with radio occultation measurements using GPS. J Geophys Res 102: 23429–23465

[6] Miller MJ (1999) Resolution studies. ECMWF Technical Memorandum No. 299: ECMWF, Reading, England

[7] Palmer PI, Barnett JJ, Eyre JR, Healy SB (2000) A non-linear optimal estimation inverse method for radio occultation measurements of temperature, humidity, and surface pressure. J Geophys Res 105(D13): 17513–17526

[8] Rodgers CD (2000) Inverse Methods for Atmospheric Sounding: Theory and Practise. In: Series on Atmospheric, Oceanic and Planetary Physics, Vol. 2: World Scientific Publ

[9] Teixeira J (1999) The impact of increased boundary layer vertical resolution on the ECMWF forecast system. ECMWF Technical Memorandum No. 268: 55 pp., ECMWF, Reading, England